### Title

NPGPx-Mediated Adaptation to Oxidative Stress Protects Motor Neurons from Degeneration in Aging by Directly Modulating O-GlcNAcase




### Journal

Cell Reports, 29(8)

### ISSN

2639-1856



### Authors

Hsieh, Yung-Lin
Su, Fang-Yi
Tsai, Li-Kai
et al.



### Publication Date

2019-11-01

### DOI

10.1016/j.celrep.2019.10.053

OPEN ACCESS
CellPress

Cell Reports
Report

# NPGPx-Mediated Adaptation to Oxidative Stress Protects Motor Neurons from Degeneration in Aging by Directly Modulating *O*-GlcNAcase

Yung-Lin Hsieh,[1,9,11] Fang-Yi Su,[1,2,11] Li-Kai Tsai,[3] Chien-Chang Huang,[1,10] Yi-Ling Ko,[1] Li-Wen Su,[1] Kai-Yun Chen,[4] Hsiu-Ming Shih,[5,6] Chun-Mei Hu,[1] and Wen-Hwa Lee[1,7,8,12,*]

[1]Genomics Research Center, Academia Sinica, Taipei 115, Taiwan
[2]Institute of Biochemistry and Molecular Biology, National Yang-Ming University, Taipei 112, Taiwan
[3]Department of Neurology, National Taiwan University Hospital, Taipei 100, Taiwan
[4]Graduate Institute of Neural Regenerative Medicine, College of Medical Science and Technology, Taipei Medical University, Taipei 110, Taiwan
[5]Institute of Biomedical Sciences, Academia Sinica, Taipei 115, Taiwan
[6]Institute of Molecular and Genomic Medicine, National Health Research Institutes, Miaoli 350, Taiwan
[7]Department of Biological Chemistry, University of California, Irvine, Irvine, CA 92697, USA
[8]Drug Development Center, China Medical University, Taichung 404, Taiwan
[9]Present address: GeneTex, Inc., Hsinchu 300, Taiwan
[10]Present address: Core Facilities for Translational Medicine, National Biotechnology Research Park, Taipei 115, Taiwan
[11]These authors contributed equally
[12]Lead Contact
*Correspondence: whlee@uci.edu
https://doi.org/10.1016/j.celrep.2019.10.053

## SUMMARY

**Amyotrophic lateral sclerosis (ALS), the most common motor neuron disease, usually occurs in middle-aged people. However, the molecular basis of age-related cumulative stress in ALS pathogenesis remains elusive. Here, we found that mice deficient in NPGPx (GPx7), an oxidative stress sensor, develop ALS-like phenotypes, including paralysis, muscle denervation, and motor neurons loss. Unlike normal spinal motor neurons that exhibit elevated *O*-GlcNAcylation against age-dependent oxidative stress, NPGPx-deficient spinal motor neurons fail to boost *O*-GlcNAcylation and exacerbate ROS accumulation, leading to cell death. Mechanistically, stress-activated NPGPx inhibits *O*-GlcNAcase (OGA) through disulfide bonding to fine-tune global *O*-GlcNAcylation. Pharmacological inhibition of OGA rescues spinal motor neuron loss in aged NPGPx-deficient mice. Furthermore, expression of *NPGPx* in ALS patients is significantly lower than in unaffected adults. These results suggest that NPGPx modulates *O*-GlcNAcylation by inhibiting OGA to cope with age-dependent oxidative stress and protect motor neurons from degeneration, providing a potential therapeutic axis for ALS.**

## INTRODUCTION

Amyotrophic lateral sclerosis (ALS) is the most common motor neuron disease (MND) and is characterized clinically by muscle wasting, leading to respiratory failure and subsequent death (Taylor et al., 2016). So far, ALS has no effective treatment, as the underlying etiological mechanism(s) remain unclear. About 90% of ALS cases are sporadic and thought to result from interactions between factors that include individual genetic predisposition, environment, and aging (Riancho et al., 2019). Indeed, aging is the most common risk factor for ALS (Mayeux, 2003) and is associated with elevated oxidative stress and cell injury. The degree of oxidative stress in aerobic organisms shifts with changes in environment, metabolism, lifestyle, and age. Therefore, aerobic organisms develop several protective mechanisms to cope with oxidative stress. Interestingly, nonselenocysteine-containing phospholipid hydroperoxide glutathione peroxidase (known as NPGPx or GPx7), which lacks a glutathione (GSH)-binding domain and peroxidase activity, serves as a redox sensor/transmitter against oxidative stress by regulating biological functions of target proteins via disulfide bond shuffling in endoplasmic reticulum (ER) (Utomo et al., 2004; Wei et al., 2012). Whether NPGPx is involved in the ALS pathogenesis remains unexplored.

*O*-GlcNAcylation is a dynamic posttranslational modification on serine or threonine residues with an *O*-linked β-N-acetylglucosamine (*O*-GlcNAc) moiety, which is regulated by *O*-GlcNAc transferase (OGT) and *O*-GlcNAcase (OGA) for addition and removal of *O*-GlcNAc, respectively (Hart, 2014; Zachara and Hart, 2004). Emerging evidence indicates that *O*-GlcNAc modification plays crucial roles in several physiological functions, including stress response (Groves et al., 2013; Hart et al., 2011; Yang and Qian, 2017). Cellular *O*-GlcNAc levels are dramatically elevated in response to oxidative stress (Champattanachai et al., 2008; Zachara et al., 2004). Increased *O*-GlcNAc levels prior to stress stimuli improve cell survival (Ngoh et al., 2009, 2011; Zachara et al., 2004), suggesting that *O*-GlcNAc modification may confer cytoprotection and cellular stress tolerance. It was also noticed that aberrant *O*-GlcNAcylation

 

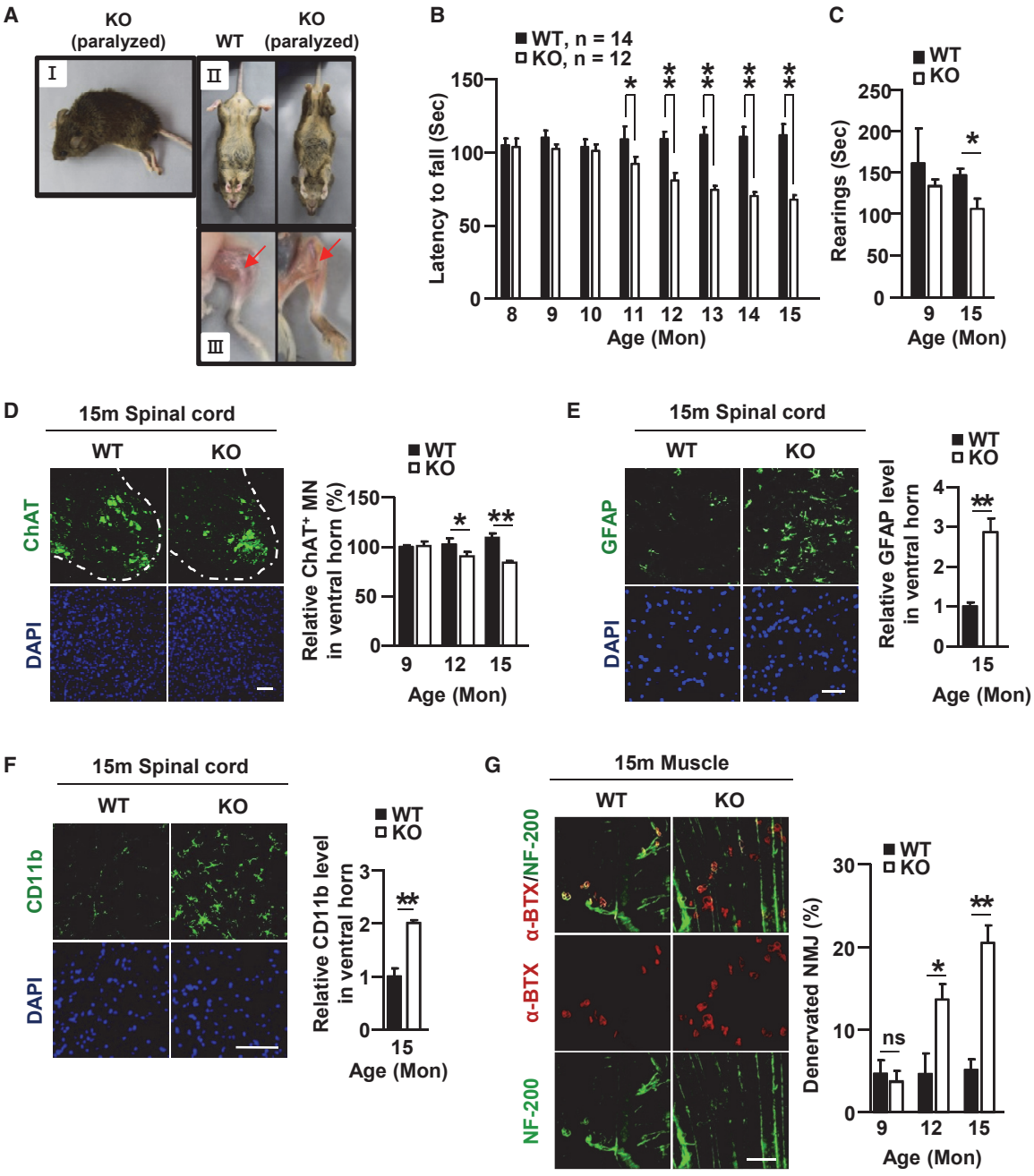


**Figure 1. NPGPx KO Mice Exhibit a Decline in Mobility and MN Degeneration**

(A) *NPGPx*$^{-/-}$ knockout (KO) mice at 13 months of age developed paralysis (I), abnormal clasping (II), and severe muscle wasting (III) in their hindlimbs compared to age-matched wild-type (WT) mice.

(B) Performance of WT (n = 14) and KO (n = 12) mice from the ages of 8 to 15 months on an accelerated rotarod apparatus.

(C) Rearing behaviors in 9- or 15-month-old WT (n = 10) and KO (n = 11) mice were monitored by the home cage system.

(D) Decreased numbers of spinal MNs in KO mice during aging. Left: representative images show ChAT (green) immunostaining of the SCs from 15-month-old mice. Right: the numbers of ChAT-stained MNs were counted, and the relative percentages of MNs were compared to that of 6-month-old WT. The white dashed lines delineate the border between white and gray matter of SCs (n = 3 mice at the indicated age).

(E and F) Increased numbers of GFAP-stained activated astrocytes (E) and CD11b-stained activated microglial cells (F) in the ventral horn of SCs from 15-month-old KO mice. Left: representative images show GFAP (E) and CD11b (F) immunostaining (green). Right: the relative fluorescence levels were compared to that of WT (n = 3 mice).

*(legend continued on next page)*

promotes neurodegenerative diseases, such as Alzheimer's disease (AD) (Yuzwa and Vocadlo, 2014). Decreased *O*-GlcNAc levels are found in neurofilament M in AD patients and in tau protein of a rat AD model (Deng et al., 2008, 2009). Consistently, *O*-GlcNAc levels are lower in the spinal cords (SCs) of ALS model animals (Lüdemann et al., 2005; Shan et al., 2012). On the other hand, neuron-specific depletion of OGT leads to impaired mobility (O'Donnell et al., 2004) or progressive neurodegeneration in mice (Lagerlöf et al., 2016; Wang et al., 2016). These observations suggest that maintaining *O*-GlcNAc homeostasis is indispensable for neuronal function and survival. However, little is known about the impact of aging on *O*-GlcNAcylation.

In this communication, we report that changes in NPGPx-mediated *O*-GlcNAcylation orchestrated by modulation of OGA activity act as an adaptive mechanism to cope with chronic oxidative-stress-targeting motor neuron (MN) degeneration in aging animals. This finding provides an intimate link between redox signaling and stress-responsive *O*-GlcNAcylation in neuronal cells.

## RESULTS

### NPGPx-Deficient Mice Develop an MN Degenerative Phenotype

NPGPx knockout (KO) (*NPGPx*$^{-/-}$) mice were generated and maintained in a C57BL/6J × 129/Ola mixed background as described in the STAR Methods. These genetic heterogeneous mice mimicking human nature population (Rivera and Tessarollo, 2008; Threadgill et al., 2011) showed advanced signs of aging (Wei et al., 2012). Approximately 10% of NPGPx KO mice at about 1 year old developed severe MND-related features, such as hindlimb paralysis, abnormal hindlimb clasping, and muscle wasting (Figure 1A). In addition, these KO mice lost choline acetyltransferase (ChAT)-positive MNs in their SCs (Figure S1A) accompanied by neuromuscular junction (NMJ) denervation in their gastrocnemius muscles (Figure S1B). This suggested that the paralysis occurring in these KO mice was due to MN degeneration.

To further assess this apparent MN degeneration, we performed rotarod testing to examine locomotor activity. KO mice exhibited significantly shorter latency to fall compared to wild-type (WT) (*NPGPx*$^{+/+}$) mice at 11 months of age, and they worsened with age (Figure 1B). Consistently, the 15-month-old KO mice also showed a reduced rearing time evaluated by home cage testing (Figure 1C), although their drinking and feeding behaviors were unaffected by NPGPx deficiency (Figure S1C). Further pathological analysis revealed that the numbers of ChAT-positive spinal MNs gradually decreased with age in the KO mice and showed about a 20% reduction at the age of 15 months compared to their WT littermates (Figure 1D). Similarly, Nissl-stained large MNs were also decreased in the SCs of 15-month-old KO mice (Figure S1D). On the other hand, the activation of glial fibrillary-associated protein (GFAP)-positive astrocytes (Figure 1E) and CD11b-positive microglia cells (Figure 1F) were increased three- and two-fold, respectively, in the SCs of 15-month-old KO mice compared to those of the WT mice. Consistently, increased NMJ denervation was also noted in the gastrocnemius muscles of NPGPx KO mice during aging (Figure 1G). About 20% of NMJs were denervated in 15-month-old KO mice, although less than 5% were in the WT littermates (Figure 1G). In contrast, the numbers of other neurons, such as COUP-TF-interacting protein 2 (Ctip2)-positive cortical MNs (Figure S1E) and Pax2-positive interneurons in the SCs (Figure S1F), were comparable between the WT and KO mice. These results demonstrated that NPGPx deficiency leads to MN degeneration in SCs and that NPGPx likely plays a protective role in guarding the survival of spinal MNs during aging.

### Loss of NPGPx Results in Failure to Boost *O*-GlcNAcylation as a Response to Age-Dependent Oxidative Stress in Spinal MNs

To explore how NPGPx has a role in spinal MN survival, we first examined the relationship between intracellular reactive oxygen species (ROS) and *O*-GlcNAc levels in SCs because increased oxidative stress and dysregulated *O*-GlcNAcylation correlated with neurodegenerative disorders (Liu et al., 2009). As shown in Figures S2A and S2B, the SCs of WT mice exhibited a considerable increase in *O*-GlcNAc levels associated with a small amount of ROS during aging, while the *O*-GlcNAc levels in brain were comparable between the ages of 9 and 15 months. In contrast, the SCs of KO mice showed limited changes in *O*-GlcNAc levels accompanied by excessive ROS accumulation during aging (Figures 2A and S2A). This significant difference in *O*-GlcNAc levels between WT and KO SCs was not observed in other organs, such as brain, muscle, pancreas, and heart (Figure S2C). Moreover, the oxidative-stress-activated signaling pathways, indicated by the levels of phosphorylation of p38 (p-p38) and eIF-2$\alpha$ (p-eIF-2$\alpha$), were also elevated with age and significantly higher in the SCs isolated from 12- and 15-month-old KO mice compared to those from WT mice (Figure 2A). These age-dependent increments in ROS and p-eIF-2$\alpha$ levels were significantly greater in ChAT-positive MNs of KO mice than in those of WT mice at the age of 15 months (Figures 2B and 2C), although the ROS levels in Ctip2-positive cortical MNs (Figure S2D) were unaffected by NPGPx deficiency. In addition, *O*-GlcNAc levels were elevated with age in ChAT-positive spinal MNs of WT mice, but not in those of KO mice (Figure 2D). Consistently, aged NPGPx-deficient mice in congenic C57BL/6J background also revealed reduced numbers of Nissl-stained spinal MNs (Figure S3A), higher p-eIF-2$\alpha$ level (Figure S3B), and reduced *O*-GlcNAc in spinal MNs (Figure S3C). These results strengthened the notion that the observed phenotypes in KO mice were mainly attributed to the deficiency of NPGPx, but not genetic background. Based on these data, NPGPx deficiency appears to cause dysregulated *O*-GlcNAcylation, which

(G) The KO mice revealed increased NMJ denervation in gastrocnemius muscle during aging. Left: representative images show the anti-Neurofilament 200 (NF-200) immunostaining and $\alpha$-bungarotoxin (BTX) labeling in the gastrocnemius muscle of 15-month-old mice. Right: the percentage of denervated NMJ increased with age in the KO, but not control, mice. >150 NMJs were counted from 3 mice at the indicated age.

Values are mean ± SEM; *$p < 0.05$, **$p < 0.01$ by two-tailed Student's t test. Scale bars represent 50 $\mu$m in (E) and 100 $\mu$m in (D), (F), and (G).

See also Figure S1.

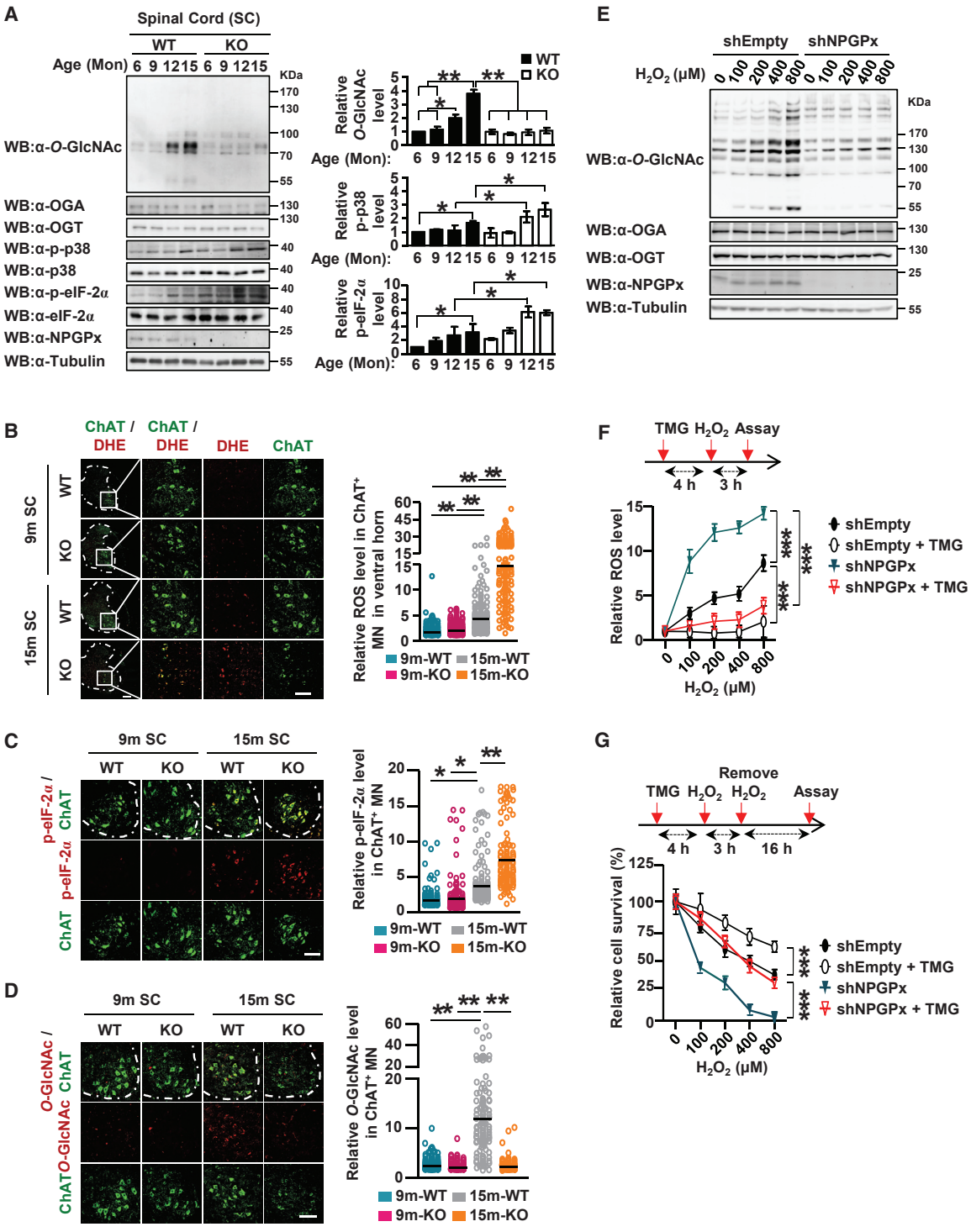


**Figure 2. NPGPx Deficiency Leads to Dysregulated *O*-GlcNAcylation Accompanied by Elevated ROS Levels in Spinal MNs during Aging**

(A) Expression levels of *O*-GlcNAcylated proteins, p-p38, and p-eIF-2α in the SCs from WT and KO mice at the indicated age. The SC lysates were immunoblotted (left) and quantified (right) as indicated (n = 3 mice).

(B–D) Left: representative images show superoxide generation detected by oxidized dihydroethidium (DHE) (red in B) and immunostaining with anti-p-eIF-2α (red in C), anti-*O*-GlcNAc (red in D), and anti-ChAT (green in B–D) in the SCs from 9- or 15-month-old mice. The white dashed lines delineate the border between white and gray matter of SCs, and the white open box in (B) indicates the enlarged regions as shown in the right column. Right: the intensity of DHE (B), p-eIF-2α (C), and *O*-GlcNAc (D) levels in ChAT-positive MN was compared to that of 9-month-old WT mice. >150 MNs from 3 mice in each group were counted.

*(legend continued on next page)*

in turn provokes increased oxidative stress damage and progressive MN death during aging.

To further confirm the link between NPGPx and *O*-GlcNAcylation in the adaption to oxidative stress, we used the MN-like NSC-34 cells depleted of NPGPx for testing *O*-GlcNAc levels in response to $H_2O_2$ treatment. Following addition of $H_2O_2$, *O*-GlcNAc levels were increased in a dose-dependent manner in control cells, but not in the NPGPx-depleted cells (Figure 2E). On the other hand, treating with Thiamet-G (TMG), an OGA inhibitor, elevated *O*-GlcNAcylation and limited $H_2O_2$-induced ROS accumulation (Figure 2F) and cell death (Figure 2G). TMG requires its target protein, OGA, to mediate the reduction of ROS, as it did not further constrain ROS levels in OGA-depleted NSC-34 cells upon $H_2O_2$ stimulation (Figures S3D and S3E). These results demonstrated that loss of NPGPx altered *O*-GlcNAcylation from levels that normally occur during oxidative stress, leading to excessive ROS accumulation and consequent death of MNs.

## Oxidative Stress Induces Formation of an NPGPx-OGA Disulfide-Bonded Complex with Reduced OGA Activity

To explore how NPGPx modulates oxidative-stress-induced *O*-GlcNAcylation in MNs, we measured the activities of the two key enzymes determining the cellular *O*-GlcNAc landscape: OGA and OGT. In NSC-34 cells, OGT activity was comparably elevated in response to $H_2O_2$ treatment in both the NPGPx-depleted and control cells (Figure S4A), while OGA activity declined over time with $H_2O_2$ treatment in the control cells, but not in the NPGPx-depleted cells (Figure S4B). The specificity of these enzymatic assays was evaluated by addition of the inhibitors alloxan (targeting OGT) and TMG (Figures S4A and S4B). Similar results were obtained with SC specimens harvested from the WT and KO mice that OGT activity was comparably elevated with age (Figure 3A), although OGA activity declined in WT SCs, but not in KO SCs, in an age-dependent manner (Figure 3B). These results suggest that NPGPx deficiency contributes to the dysregulated OGA activity for modulating *O*-GlcNAcylation in MNs.

To test how NPGPx directly modulates OGA activity upon oxidative stress, we first examined the interaction between NPGPx and OGA in SCs from aged mice because they accumulated ROS. As shown in Figure 3C, the co-immunoprecipitated (coIP) complex of NPGPx and OGA was clearly detected in the SCs of 15-month-old mice but barely detectable in those from 9-month-old mice. Consistently, the complex was barely detectable in NSC-34 cells grown in normal conditions (Figures S4C and S4D, lane 2), although it was significantly increased in cells treated with $H_2O_2$ (Figures S4C and S4D). Furthermore, the specific interaction between NPGPx and OGA was confirmed by proximal ligation assay (PLA), as the co-localization of these two proteins increased with $H_2O_2$ treatment in the calnexin-stained ER of NSC-34 cells (Figure S4E). These results indicated that ROS accumulation promotes NPGPx interaction with OGA in MNs.

It is known that NPGPx uses its cysteine (Cys) residues, Cys57 and Cys86, to interact with its target proteins (Wei et al., 2012). To test whether NPGPx interacts with OGA in a similar manner, we performed coIP experiments using 293T cells ectopically expressing OGA and WT ($NPGPx^{WT}$) or Cys-mutated NPGPx ($NPGPx^{CS}$ or $NPGPx^{CA}$), of which Cys57 and Cys86 were substituted with Ser or Ala, respectively. With $H_2O_2$ treatment, complex formation was increased in cells expressing $NPGPx^{WT}$ and OGA, although the complex was undetectable in cells expressing $NPGPx^{CS}$ or $NPGPx^{CA}$ mutant (Figures 3D, 3E, and S4F), suggesting the crucial roles of these Cys residues in their interaction. To test whether NPGPx interacts with OGA through disulfide bonding, we analyzed the complexes by non-reducing SDS-PAGE. With $H_2O_2$ treatment, OGA formed high-molecular-weight (HMW) complexes with $NPGPx^{WT}$, but not $NPGPx^{CS}$, under non-reducing conditions (Figure 3E). To further examine whether NPGPx directly complexes with OGA, we modulated the redox state of recombinant OGA and NPGPx by treating with $H_2O_2$ or a reducing agent and performed an *in vitro* complex formation assay. It was found that the oxidized $NPGPx^{WT}$ ($oNPGPx^{WT}$) formed HMW complexes with oxidized OGA (oOGA), but not reduced OGA (rOGA), in a Cys-dependent manner (Figure 3F, left). Moreover, these HMW complexes were abolished when the reducing agent was introduced into the SDS-PAGE analysis (Figure 3F, right), indicating that the direct interaction between NPGPx and OGA occurred through covalent disulfide bonding. In contrast, OGT was not an NPGPx-binding partner because no association was detected either by the HMW-complex formation assay or the glutathione S-transferase (GST) pull-down assay (Figures S4G and S4H). Taken together, these findings showed that oxidative stress triggers formation of a disulfide-bonded complex between NPGPx and OGA.

To address whether the complex formation with NPGPx affects OGA function, we performed both *in vitro* and *in vivo* OGA activity assays. OGA activity was suppressed by $oNPGPx^{WT}$, but not $oNPGPx^{CS}$, in a dose-dependent manner *in vitro*, although this suppression was abolished by addition of the reducing agent (Figure 3G). Furthermore, such suppression of OGA activity was only found when using $oNPGPx^{WT}$, but not the $NPGPx^{CS}$ mutant or reduced $NPGPx^{WT}$ ($rNPGPx^{WT}$) (Figure S4I). To further confirm the role of NPGPx in *in vivo* OGA activity, we employed the NPGPx-depleted NSC-34 cells reconstituted with ectopically expressed $NPGPx^{WT}$ or $NPGPx^{CS}$. Consistently, in $NPGPx^{WT}$-reconstituted, but not $NPGPx^{CS}$-reconstituted, cells, OGA activity was significantly reduced with $H_2O_2$ treatment (Figure 3I). This difference was not due to

(E) Immunoblotting showing the *O*-GlcNAc levels in control (shEmpty) and NPGPx-depleted (shNPGPx) NSC-34 cells upon $H_2O_2$ stimulation. The cells were treated with the indicated concentration of $H_2O_2$ for 3 h and harvested for immunoblotting as indicated.

(F and G) Effects of $H_2O_2$ and TMG treatment on cellular ROS levels measured by CM-$H_2$DCFDA labeling assay (F) and cell viability measured by XTT assay (G) of control and NPGPx-depleted NSC-34 cells. $H_2O_2$-untreated cells were used as the control for normalization.

Values are mean ± SD in (A), (F), and (G) and mean ± SEM in (B)–(D). *$p < 0.05$, **$p < 0.01$ by two-tailed Student's t test in (A), Welch's t test in (B)–(D), and two-way ANOVA in (F) and (G). Scale bars represent 100 μm.

See also Figures S2 and S3.

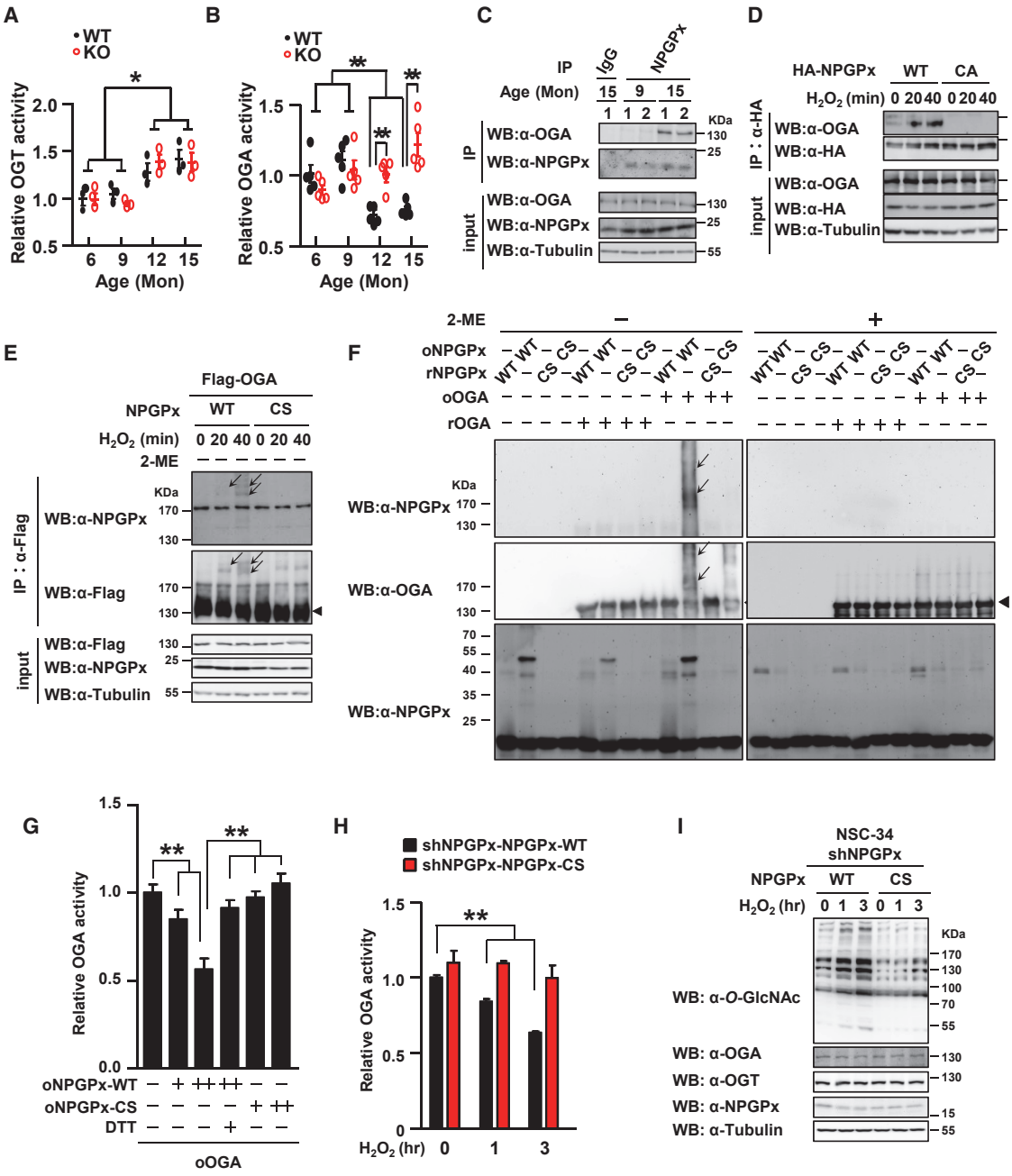


**Figure 3. Oxidative Stress Promotes NPGPx to Form a Disulfide-Bonded Complex with OGA for Suppressing Its Activity and Consequently Elevating *O*-GlcNAcylation**

(A and B) Enzymatic activity of OGT (A; n = 3 per group) and OGA (B; n = 5 per group) in the SCs of WT and KO mice at the indicated age. The activity assays were performed in triplicate. The averaged activity of SC of 6-month-old WT mice was used as the control for normalization.

(C) Association of NPGPx and OGA by coIP assay was increased in an age-dependent manner. The SC lysates from 9- or 15-month-old mice (n = 2 per group) were used for IP with anti-NPGPx and then subjected to western blotting.

(D) Cysteine residue (Cys)-dependent interaction between NPGPx and OGA. WT or Cys-to-Ala (CA) mutated hemagglutinin (HA)-NPGPx and OGA were ectopically co-expressed in 293T cells. The cells were treated with 800 μM $H_2O_2$ for the indicated time periods. The cell lysates were used for IP with HA beads and then subjected to western blotting.

(E) NPGPx forms disulfide-bond-dependent complexes with OGA in cells with $H_2O_2$ stimulation. WT or Cys-to-Ser (CS) mutated NPGPx and FLAG-OGA were ectopically co-expressed in 293T cells that were treated with 800 μM $H_2O_2$ for the indicated time periods. The cell lysates were used for IP with M2 beads and then subjected to SDS-PAGE under non-reducing conditions (without 2-mercaptoethanol [2-ME]) followed by immunoblotting.

*(legend continued on next page)*

unequal expression levels of OGA and NPGPx in the cells (Figure S4J), supporting the notion that NPGPx mediated OGA functions through posttranslational modification. Moreover, $H_2O_2$ treatment provoked *O*-GlcNAcylation in $NPGPx^{WT}$-reconstituted cells, but not $NPGPx^{CS}$-reconstituted cells (Figure 3J). Thus, NPGPx promotes *O*-GlcNAcylation through inhibiting OGA activity to cope with oxidative stress.

### Thiamet-G Treatment Improves the MN Degeneration in NPGPx KO Mice, and Human ALS Patients Express Lower Levels of NPGPx

To test whether increasing *O*-GlcNAcylation improves survival of spinal MNs during aging, we treated the aged KO mice with TMG and observed a significantly elevation of *O*-GlcNAc levels in their SCs (Figure 4A). Furthermore, we found that the KO mice treated with TMG for 3 months significantly improved in locomotor activity (Figure 4B), and the numbers of ChAT-positive MNs in their SCs were increased as well as the oxidative stress levels were reduced (Figures 4C and 4D). Importantly, the NMJ architecture in the gastrocnemius muscles of KO mice was partially rescued by TMG treatment when compared to the untreated KO mice (Figure 4E). These results strongly suggested that elevating *O*-GlcNAcylation through suppressing OGA activity lessens MN degeneration in the KO mice.

Because MN degeneration is a major feature of human ALS, it is reasonable to deduce that human ALS patients may express NPGPx abnormally. To address this, we analyzed peripheral blood mononuclear cells (PBMCs) from 33 ALS patients and 21 age-matched healthy controls (Figure S5) and found that *NPGPx* expression levels measured by quantitative RT-PCR (qRT-PCR) were significantly lower in the PBMCs from ALS patients (Figure 4F). This result argued for the potential clinical significance of NPGPx in ALS.

## DISCUSSION

Oxidative stress manifests from increased free radical production and/or compromised antioxidant mechanisms in cells. Interestingly, the composition of neuronal tissue is rich in polyunsaturated fatty acids, which is predisposed to peroxidation and oxidative modification. Thus, the CNS is particularly sensitive to oxidative stress, which is thought to be a common culprit in various neurodegenerative diseases, including ALS (Mattson and Magnus, 2006; Uttara et al., 2009). Accordingly, an understanding of how neuronal cells defend themselves from oxidative stress is crucial for unraveling the etiologic mystery of these diseases. In this communication, we elucidated a mechanism of how NPGPx mediates an oxidative stress adaption to protect spinal MNs from degeneration during aging. As illustrated in the model (Figure 4G), the dynamic balance between OGT and OGA in *O*-GlcNAcylation represents cellular homeostasis in normal MNs. With age-dependent ROS accumulation, the stress sensor NPGPx transmits an oxidative signal to its target enzyme, OGA, through formation of a disulfide-bonded complex to curb OGA's enzymatic activity and elevate *O*-GlcNAcylation against oxidative stress. In the NPGPx-deficient MNs, the OGA activity is unrestrained, resulting in impaired *O*-GlcNAcylation accompanied by elevated ROS accumulation and MN degeneration.

The mechanistic connections between *O*-GlcNAcylation, oxidative stress releasing, and neuronal cell survival are demonstrated herein. Importantly, the *O*-GlcNAc cycling enzymes appear to play a crucial role in modulating cellular *O*-GlcNAcylation for MN survival as the impaired *O*-GlcNAcylation due to lack of NPGPx-mediated OGA regulation was restored by TMG treatment, which in turn reduced oxidative stress and prevented MN death in KO SCs (Figure 4). Notably, the expression levels of the *O*-GlcNAc cycling enzymes were similar between the WT and KO cells, indicating that the posttranslational modification of these enzymes could be compromised by NPGPx deficiency. Interestingly, oNPGPx formed a disulfide-bonded complex with oOGA to suppress its enzymatic activity, but not rOGA (Figure 3F), asserting that the oxidation of OGA acts as a "priming signal" for coupling with NPGPx to establish this negative feedback regulation. This is consistent with the observation that thiol-reactive compounds could inactivate OGA activity (Dong and Hart, 1994; Kim et al., 2007), supporting the crucial role of the Cys residues in its functional regulation.

Intriguingly, MNs in the SCs of the KO mice suffered more damage than brain MNs. This was supported by the observation that spinal MNs exhibited higher ROS levels than cortical MNs (Figures 2B and S2D). Moreover, the difference in *O*-GlcNAc regulatory machinery between SCs and brain was quite obvious as the *O*-GlcNAc levels in the SCs elevated gradually with age, although this was not the case in the brain (Figures 2A and S2B). At 6 months of age, the brain revealed higher *O*-GlcNAc levels than the SCs in mice. At 15 months of age, the *O*-GlcNAc levels were comparable between the two organs (Figure S2B). This observation is consistent with a previous report that the

(F) *In vitro* disulfide-bonded complex formation assay. Recombinant NPGPx and OGA proteins were oxidized by $H_2O_2$ or reduced by Tris(2-carboxyethyl) phosphine (TCEP), respectively, and then subjected to the protein binding assay followed by SDS-PAGE analysis with or without reducing agent (2-ME). The arrowheads indicate the NPGPx-OGA complexes, and the triangle indicates OGA in monomeric form. o, oxidized; r, reduced.

(G) Oxidized NPGPx suppressed OGA enzymatic activity in a disulfide-bond-dependent manner. oOGA at 1 μM was incubated with 20 (+) or 40 (++) μM oNPGPx WT or CS mutant in a solution containing reducing agent (100 mM DTT) or not for 2 h and then subjected to OGA activity assay. The activity of oOGA alone was used as a control for normalization. The activity assays were performed in triplicate.

(H) OGA activity was suppressed by WT-, but not CS-mutated NPGPx upon $H_2O_2$ treatment. NSC-34 cells depleted by shNPGPx and then reconstituted with human WT- or CS-mutated NPGPx were treated with 800 μM $H_2O_2$ for the indicated time periods. The whole-cell lysates were harvested for OGA activity assay. The OGA activity of hNPGPx WT-reconstituted cells without $H_2O_2$ treatment was used as a control for normalization. The activity assays were performed in triplicate.

(I) Immunoblotting showing the *O*-GlcNAcylated proteins, OGA, OGT, NPGPx, and tubulin in human WT or CS mutated NPGPx-reconstituted NSC-34 shNPGPx cells treated with 800 μM $H_2O_2$ for the indicated time periods.

Values are mean ± SEM in (A) and (B) and mean ± SD in (G) and (H). *$p < 0.05$, **$p < 0.01$ by two-tailed Student's t test.

See also Figure S4.

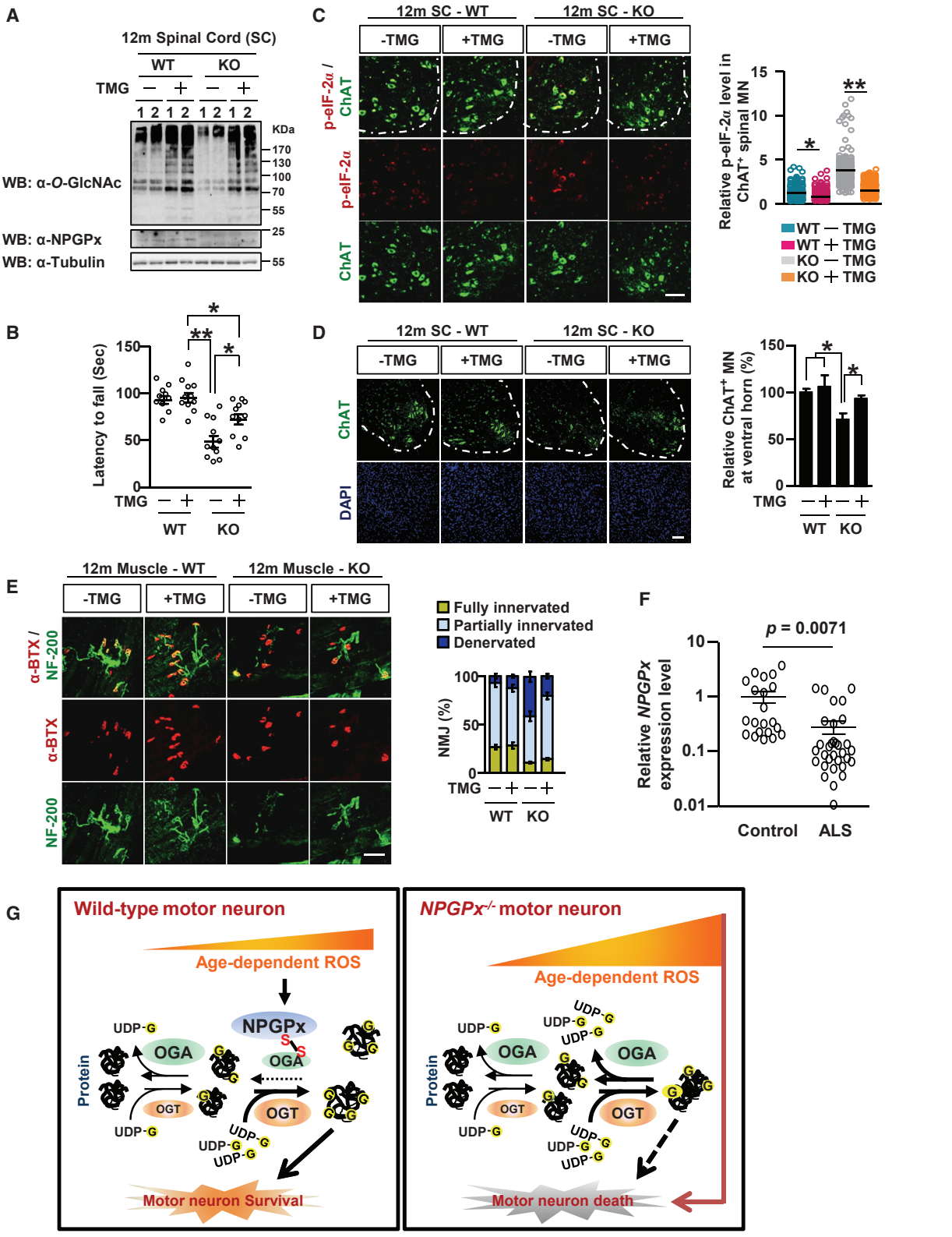


*(legend on next page)*

rat brain exhibits steady *O*-GlcNAc levels after sexual maturation until 2 years of age (Liu et al., 2012). Furthermore, the expression levels of *O*-GlcNAc cycling enzymes are higher in the brain than in the SCs (Figure S2B). These results suggest that the brain maintains more efficient *O*-GlcNAc regulatory machinery and higher *O*-GlcNAc levels compared to the SCs, providing a better "buffering" zone to fend off stress and protect its function. These differences between the two organs may explain why the SC is the most affected region of the CNS in NPGPx-deficient mice.

Though all GPxs have roles in redox homeostasis, the stress sensing/transferring and noncatalytic characteristics of NPGPx are quite distinct from other GPx members that utilize GSH to catalyze the reduction of $H_2O_2$ to water (Brigelius-Flohé and Maiorino, 2013). It was noted that conditional ablation of GPx4, a phospholipid GPx, in neurons of mice contributed to rapid MN degeneration and paralysis (Chen et al., 2015). However, NPGPx KO mice exhibited gradual loss of spinal MNs with age, which closely mimics human ALS disease progression. Indeed, low *NPGPx* expression was observed in human PBMCs derived from ALS patients (Figure 4E). Thus, elucidating the etiologic mechanism of MN degeneration in NPGPx-deficient mice offers innovative insights into potential strategies for managing this relentless disease.

## STAR★METHODS

Detailed methods are provided in the online version of this paper and include the following:

- KEY RESOURCES TABLE
- LEAD CONTACT AND MATERIALS AVAILABILITY
- EXPERIMENTAL MODEL AND SUBJECT DETAILS
  - Ethics Statement
  - Human Specimens
  - Animal protocols, generation of NPGPx-deficient mice, and mouse Thiamet-G treatment
  - Sample size estimation
  - General cell culture, lentiviral infection, and plasmid transfection
- METHOD DETAILS
  - Animal rotarod test and home cage analysis
  - Plasmids and construction of expression plasmids
  - Tissue preservation, immunohistochemistry, and image analysis
  - Nissl staining
  - Generation of NPGPx-specific monoclonal antibody
  - *In situ* proximity ligation assay
  - Enzymatic activity assay
  - Co-immunoprecipitation (Co-IP) and Western analysis
  - Recombinant protein preparation and *in vitro* protein binding assay
  - ROS level measurement *in vitro* and *in vivo*
  - Cell viability assay
  - RNA extraction, reverse transcription and real-time qPCR
  - Experiment design
- QUANTIFICATION AND STATISTICAL ANALYSIS
  - Statistical Analyses
- DATA AND CODE AVAILABILITY

### SUPPLEMENTAL INFORMATION

Supplemental Information can be found online at https://doi.org/10.1016/j.celrep.2019.10.053.

### ACKNOWLEDGMENTS

We are grateful to Drs. Alex Ball and Chun-Kai Huang for critical reading of the manuscript. We thank NRPB Core Facility for providing lentivirus constructs of NPGPx shRNA and the Taiwan Mouse Clinic for performing rotarod and home-cage behavior experiments. This research work was supported by funds from Academia Sinica, Taiwan, and grants from Ministry of Science and Technology, Taiwan (MOST 104-0210-01-09-02, MOST 105-0210-01-13-01, and MOST 106-0210-01-15-02), higher education sprout project by the Ministry of Education, Taiwan, and funds from Philips Morris Foundation, USA.

### AUTHOR CONTRIBUTIONS

Y.-L.H., F.-Y.S., L.-K.T., H.-M.S., C.-M.H., and W.-H.L. designed the study. L.-K.T. and K.-Y.C. collected ALS patients' samples. Y.-L.H., F.-Y.S.,

**Figure 4. Elevated *O*-GlcNAcylation by TMG Treatment Decreases Spinal MN Degeneration in Aged NPGPx Knockout Mice, and ALS Patients Express Lower *NPGPx* mRNA**

(A) Elevated *O*-GlcNAcylation in SCs with TMG treatment. Two pairs of 12-month-old WT and KO mice were treated with or without TMG orally (100 mg/kg) for 12 h. Their lumbar SCs were harvested for immunoblotting as indicated.

(B) TMG treatment rescued the locomotor activity of aged KO mice analyzed by accelerated rotarod tests. Ten or eleven pairs of WT and KO mice were treated with or without TMG orally (100 mg/kg) from the ages of 9 to 12 months.

(C) TMG treatment downregulated p-eIF-2α levels in spinal MN. Left: representative images show p-eIF-2α (red) and ChAT (green) immunostaining in SC of 12-month-old mice with or without TMG treatment. Right: the intensity of p-eIF-2α level in ChAT-positive MNs was compared to that of TMG-untreated WT. >150 MNs from 3 mice in each group were counted.

(D) The numbers of MNs in the SCs of aged KO mice were rescued by TMG treatment. Left: representative images show ChAT (green) immunostaining in the SCs of 12-month-old mice with or without TMG treatment. Right: the quantification of ChAT-positive MNs is shown. The TMG-untreated WT was used as a control for normalization (n = 4 mice).

(E) TMG treatment partially rescued the denervation of NMJ in KO mice. Left: representative images show the NMJ architecture in the gastrocnemius muscles of 12-month-old mice with or without TMG treatment. Right: the percentage of completely denervated NMJs decreased in the KO mice treated with TMG. >150 NMJs were counted from 3 mice at the indicated group.

(F) Expression levels of *NPGPx* in PBMCs from ALS patients (n = 33) and unaffected controls (n = 21) were determined by quantitative RT-PCR.

(G) Proposed model of NPGPx-mediated spinal stress adaptation in aging.

Values are mean ± SEM in (B)–(D) and mean ± SD in (F). *$p < 0.05$, **$p < 0.01$ by two-tailed Student's t test in (B) and Welch's t test in (C), (D), and (F). In (C) and (D), the white dashed lines delineate the border between white and gray matter of SCs. Scale bars represent 100 μm.

See also Figure S5.

C.-C.H., Y.-L.K., and L.-W.S. conducted experiments. Y.-L.H., F.-Y.S., L.-K.T., and W.-H.L. wrote the manuscript.

## DECLARATION OF INTERESTS

The authors declare no competing interests.

Received: April 3, 2019
Revised: July 10, 2019
Accepted: October 11, 2019
Published: November 19, 2019

## REFERENCES

Brigelius-Flohé, R., and Maiorino, M. (2013). Glutathione peroxidases. Biochim. Biophys. Acta Gen. Subj. *1830*, 3289–3303.

Cashman, N.R., Durham, H.D., Blusztajn, J.K., Oda, K., Tabira, T., Shaw, I.T., Dahrouge, S., and Antel, J.P. (1992). Neuroblastoma x spinal cord (NSC) hybrid cell lines resemble developing motor neurons. Dev. Dyn. *194*, 209–221.

Champattanachai, V., Marchase, R.B., and Chatham, J.C. (2008). Glucosamine protects neonatal cardiomyocytes from ischemia-reperfusion injury via increased protein *O*-GlcNAc and increased mitochondrial Bcl-2. Am. J. Physiol. Cell Physiol. *294*, C1509–C1520.

Chen, L., Hambright, W.S., Na, R., and Ran, Q. (2015). Ablation of the ferroptosis inhibitor glutathione peroxidase 4 in neurons results in rapid motor neuron degeneration and paralysis. J. Biol. Chem. *290*, 28097–28106.

Deng, Y., Li, B., Liu, F., Iqbal, K., Grundke-Iqbal, I., Brandt, R., and Gong, C.X. (2008). Regulation between *O*-GlcNAcylation and phosphorylation of neurofilament-M and their dysregulation in Alzheimer disease. FASEB J. *22*, 138–145.

Deng, Y., Li, B., Liu, Y., Iqbal, K., Grundke-Iqbal, I., and Gong, C.X. (2009). Dysregulation of insulin signaling, glucose transporters, *O*-GlcNAcylation, and phosphorylation of tau and neurofilaments in the brain: Implication for Alzheimer's disease. Am. J. Pathol. *175*, 2089–2098.

Dong, D.L., and Hart, G.W. (1994). Purification and characterization of an *O*-GlcNAc selective N-acetyl-beta-D-glucosaminidase from rat spleen cytosol. J. Biol. Chem. *269*, 19321–19330.

Groves, J.A., Lee, A., Yildirir, G., and Zachara, N.E. (2013). Dynamic *O*-GlcNAcylation and its roles in the cellular stress response and homeostasis. Cell Stress Chaperones *18*, 535–558.

Hart, G.W. (2014). Three decades of research on *O*-GlcNAcylation - a major nutrient sensor that regulates signaling, transcription and cellular metabolism. Front. Endocrinol. (Lausanne) *5*, 183.

Hart, G.W., Slawson, C., Ramirez-Correa, G., and Lagerlof, O. (2011). Cross talk between *O*-GlcNAcylation and phosphorylation: roles in signaling, transcription, and chronic disease. Annu. Rev. Biochem. *80*, 825–858.

Huang, Y.S., Chang, C.C., Huang, T.C., Hsieh, Y.L., and Shih, H.M. (2012). Daxx interacts with and modulates the activity of CREB. Cell Cycle *11*, 99–108.

Kim, E.J., Amorelli, B., Abdo, M., Thomas, C.J., Love, D.C., Knapp, S., and Hanover, J.A. (2007). Distinctive inhibition of *O*-GlcNAcase isoforms by an alpha-GlcNAc thiolsulfonate. J. Am. Chem. Soc. *129*, 14854–14855.

Lagerlöf, O., Slocomb, J.E., Hong, I., Aponte, Y., Blackshaw, S., Hart, G.W., and Huganir, R.L. (2016). The nutrient sensor OGT in PVN neurons regulates feeding. Science *351*, 1293–1296.

Liu, F., Shi, J., Tanimukai, H., Gu, J., Gu, J., Grundke-Iqbal, I., Iqbal, K., and Gong, C.X. (2009). Reduced *O*-GlcNAcylation links lower brain glucose metabolism and tau pathology in Alzheimer's disease. Brain *132*, 1820–1832.

Liu, Y., Li, X., Yu, Y., Shi, J., Liang, Z., Run, X., Li, Y., Dai, C.L., Grundke-Iqbal, I., Iqbal, K., et al. (2012). Developmental regulation of protein *O*-GlcNAcylation, *O*-GlcNAc transferase, and *O*-GlcNAcase in mammalian brain. PLoS ONE *7*, e43724.

Lüdemann, N., Clement, A., Hans, V.H., Leschik, J., Behl, C., and Brandt, R. (2005). *O*-glycosylation of the tail domain of neurofilament protein M in human neurons and in spinal cord tissue of a rat model of amyotrophic lateral sclerosis (ALS). J. Biol. Chem. *280*, 31648–31658.

Mattson, M.P., and Magnus, T. (2006). Ageing and neuronal vulnerability. Nat. Rev. Neurosci. *7*, 278–294.

Mayeux, R. (2003). Epidemiology of neurodegeneration. Annu. Rev. Neurosci. *26*, 81–104.

Ngoh, G.A., Hamid, T., Prabhu, S.D., and Jones, S.P. (2009). *O*-GlcNAc signaling attenuates ER stress-induced cardiomyocyte death. Am. J. Physiol. Heart Circ. Physiol. *297*, H1711–H1719.

Ngoh, G.A., Watson, L.J., Facundo, H.T., and Jones, S.P. (2011). Augmented *O*-GlcNAc signaling attenuates oxidative stress and calcium overload in cardiomyocytes. Amino Acids *40*, 895–911.

O'Donnell, N., Zachara, N.E., Hart, G.W., and Marth, J.D. (2004). Ogt-dependent X-chromosome-linked protein glycosylation is a requisite modification in somatic cell function and embryo viability. Mol. Cell. Biol. *24*, 1680–1690.

Riancho, J., Gonzalo, I., Ruiz-Soto, M., and Berciano, J. (2019). Why do motor neurons degenerate? Actualization in the pathogenesis of amyotrophic lateral sclerosis. Neurologia *34*, 27–37.

Rivera, J., and Tessarollo, L. (2008). Genetic background and the dilemma of translating mouse studies to humans. Immunity *28*, 1–4.

Shan, X., Vocadlo, D.J., and Krieger, C. (2012). Reduced protein *O*-glycosylation in the nervous system of the mutant SOD1 transgenic mouse model of amyotrophic lateral sclerosis. Neurosci. Lett. *516*, 296–301.

Taylor, J.P., Brown, R.H., Jr., and Cleveland, D.W. (2016). Decoding ALS: from genes to mechanism. Nature *539*, 197–206.

Threadgill, D.W., Miller, D.R., Churchill, G.A., and de Villena, F.P.M. (2011). The collaborative cross: a recombinant inbred mouse population for the systems genetic era. ILAR J. *52*, 24–31.

Utomo, A., Jiang, X., Furuta, S., Yun, J., Levin, D.S., Wang, Y.C., Desai, K.V., Green, J.E., Chen, P.L., and Lee, W.H. (2004). Identification of a novel putative non-selenocysteine containing phospholipid hydroperoxide glutathione peroxidase (NPGPx) essential for alleviating oxidative stress generated from polyunsaturated fatty acids in breast cancer cells. J. Biol. Chem. *279*, 43522–43529.

Uttara, B., Singh, A.V., Zamboni, P., and Mahajan, R.T. (2009). Oxidative stress and neurodegenerative diseases: a review of upstream and downstream antioxidant therapeutic options. Curr. Neuropharmacol. *7*, 65–74.

Wang, A.C., Jensen, E.H., Rexach, J.E., Vinters, H.V., and Hsieh-Wilson, L.C. (2016). Loss of *O*-GlcNAc glycosylation in forebrain excitatory neurons induces neurodegeneration. Proc. Natl. Acad. Sci. USA *113*, 15120–15125.

Wei, P.C., Hsieh, Y.H., Su, M.I., Jiang, X., Hsu, P.H., Lo, W.T., Weng, J.Y., Jeng, Y.M., Wang, J.M., Chen, P.L., et al. (2012). Loss of the oxidative stress sensor NPGPx compromises GRP78 chaperone activity and induces systemic disease. Mol. Cell *48*, 747–759.

Yang, X., and Qian, K. (2017). Protein *O*-GlcNAcylation: emerging mechanisms and functions. Nat. Rev. Mol. Cell Biol. *18*, 452–465.

Yuzwa, S.A., and Vocadlo, D.J. (2014). *O*-GlcNAc and neurodegeneration: biochemical mechanisms and potential roles in Alzheimer's disease and beyond. Chem. Soc. Rev. *43*, 6839–6858.

Zachara, N.E., and Hart, G.W. (2004). *O*-GlcNAc a sensor of cellular state: the role of nucleocytoplasmic glycosylation in modulating cellular function in response to nutrition and stress. Biochim. Biophys. Acta *1673*, 13–28.

Zachara, N.E., O'Donnell, N., Cheung, W.D., Mercer, J.J., Marth, J.D., and Hart, G.W. (2004). Dynamic *O*-GlcNAc modification of nucleocytoplasmic proteins in response to stress. A survival response of mammalian cells. J. Biol. Chem. *279*, 30133–30142.

## STAR★METHODS

### KEY RESOURCES TABLE

| REAGENT or RESOURCE | SOURCE | IDENTIFIER |
|---|---|---|
| Antibodies for western blot | | |
| OGA | Sigma-Aldrich | Cat# SAB4200267; RRID:AB_10797267 |
| OGA | Sigma-Aldrich | Cat# SAB4200311; RRID:AB_10898726 |
| OGT (DM-17) | Sigma-Aldrich | Cat# O6264; RRID:AB_532313 |
| p38 | Cell Signaling Technology | Cat# 9212; RRID:AB_330713 |
| phospho-p38 | Cell Signaling Technology | Cat# 9211; RRID:AB_331641 |
| eIF-2α | Cell Signaling Technology | Cat# 9722; RRID:AB_2230924 |
| NPGPx | GeneTex | Cat# GTX108578; RRID:AB_2037098 |
| α-tubulin | GeneTex | Cat# GTX11302; RRID:AB_381291 |
| Flag | Sigma-Aldrich | Cat# F3165; RRID:AB_259529 |
| HA | Covance | Cat# MMS-101; PRRID:AB_2314672 |
| GST | GeneTex | Cat# GTX110736; RRID:AB_1949427 |
| Antibodies for immunohistochemistry | | |
| Choline acetyltransferase (ChAT) | Merck Millipore | Cat# AB144P; RRID:AB_2079751 |
| Glial fibrillary-associated protein (GFAP) | Agilent | Cat# Z0334; RRID:AB_10013382 |
| CD11b | BioLegend | Cat# 101201; RRID:AB_312784 |
| COUP-TF-interacting protein 2 (Ctip2) | Abcam | Cat# ab18465; RRID:AB_10015215 |
| Neurofilament 200 (NF-200) | Abcam | Cat# ab8135; RRID:AB_306298 |
| Ubiquitin | Abcam | Cat# ab7780; RRID:AB_306069 |
| Bungarotoxin (BTX), Alexa Fluor 594 conjugate | Invitrogen | Cat# B-13423; RRID:AB_2802145 |
| Calnexin | Abcam | Cat# ab192439; RRID:AB_2802157 |
| Paired box gene 2 (Pax2) | Abcam | Cat# ab79389; RRID:AB_1603338 |
| NPGPx (clone 7E7-3B2) | This paper | N/A |
| Antibodies for both western blot and immunohistochemistry | | |
| *O*-GlcNAc (CTD110.6) | Cell Signaling Technology | Cat# 9875; RRID:AB_10950973 |
| phospho-eIF-2α | Cell Signaling Technology | Cat# 3597; RRID:AB_390740 |
| Antibodies for immunoprecipitation assay | | |
| Anti-Flag® M2 affinity gel | Sigma-Aldrich | Cat# A2220; RRID:AB_10063035 |
| Monoclonal Anti-HA–Agarose antibody produced in mouse | Sigma-Aldrich | Cat# A2095; RRID:AB_257974 |
| Reagents for proximity ligation assay | | |
| PLA® probe anti-mouse MINUS | Sigma-Aldrich | Cat# DUO92004 |
| PLA® Probe Anti-Rabbit PLUS | Sigma-Aldrich | Cat# DUO92002 |
| Duolink® *In Situ* Detection Reagents FarRed | Sigma-Aldrich | Cat# DUO92013 |
| Chemicals | | |
| Thiamet-G | Carbosynth | MD08856 |
| Sodium phosphate | Sigma-Aldrich | Cat# 342483 |
| NaCl | Sigma-Aldrich | Cat# S7653 |
| EDTA | Sigma-Aldrich | Cat# EDS |
| NP-40 | Sigma-Aldrich | Cat# NP40S |
| SDS | Sigma-Aldrich | Cat# L6026 |
| Deoxycholic acid | Sigma-Aldrich | Cat# 30960 |
| Proteinase inhibitor mixture | Roche | Cat# 4693132001 |
| Phosphatase inhibitor cocktail | Tools | Cat# TARR-WBC1 |
| BSA | Sigma-Aldrich | Cat# 05470 |

(*Continued on next page*)

*Continued*

| REAGENT or RESOURCE | SOURCE | IDENTIFIER |
|---|---|---|
| Triton X-100 | Sigma-Aldrich | Cat# X100 |
| AMP | Sigma-Aldrich | Cat# 01930 |
| $MgCl_2$ | Sigma-Aldrich | Cat# M2670 |
| HEPES | Sigma-Aldrich | Cat# H4034 |
| Tris-HCl | Sigma-Aldrich | Cat# T5941 |
| para-Nitrophenyl-N-acetyl-β-D-GlcNAc | Sigma-Aldrich | Cat# N9376 |
| GalNAc | Sigma-Aldrich | Cat# A2795 |
| Sodium carbonate | Sigma-Aldrich | Cat# S7795 |
| IPTG | Sigma-Aldrich | Cat# I6758 |
| Glycerol | Sigma-Aldrich | Cat# G5516 |
| $H_2O_2$ | Sigma-Aldrich | Cat# H1009 |
| CM-$H_2$DCFDA | Invitrogen | Cat# C6827 |
| Dihydroethidium (DHE) | Invitrogen | Cat# D11347 |
| TransIT-LT1 | Mirus Bio | Cat# MIR2300 |
| Ni Sepharose 6 Fast flow | GE Healthcare | Cat# 17-5318-02 |
| Glutathione agarose | Thermo Fisher Scientific Inc. | Cat# 16100 |
| Tris(2-carboxyethyl)phosphine (TCEP) | Sigma-Aldrich | Cat# 646547 |
| UDP-[$^3$H]-GlcNAc | PerkinElmer | Cat# NET434250UC |
| Cresyl Violet acetate | Sigma | Cat# C5042 |
| Ficoll®-Paque Premium | GE Healthcare | Cat# GE17-5442-02 |
| Recombinant DNAs | | |
| pLKO-AS1 | National RNAi Core Facility | N/A (discontinued) |
| pLKO.1-shLuc | National RNAi Core Facility | N/A (discontinued) |
| pLKO.1-shNPGPx (mouse) | National RNAi Core Facility | TRCN0000076564 |
| pLKO.1-shOGA (mouse) | National RNAi Core Facility | TRCN0000248909 |
| pLAS3w.Pbsd-L-tRFP | National RNAi Core Facility | Service ID: C6-8-46 |
| pLAS3w-human NPGPx (WT or C2S2) | This paper | N/A |
| pcDNA3.0-HA | Invitrogen | N/A (discontinued) |
| pcDNA3.0-HA-human NPGPx (WT or C2A2) | This paper | N/A |
| p3xFlag-CMV™ 7.1 | Sigma-Aldrich | Cat# E7533 |
| pCMV-3xFlag-human OGA | This paper | N/A |
| pET48-TEV-human NPGPx (WT or C2S2, a.a. 19-187) | Wei et al., 2012 | N/A |
| pET15b | Merck Millipore | Cat# 69661 |
| pET15b-human OGA | This paper | N/A |
| pGEX-4T-2 | GE Healthcare | Cat# GE28-9545-50 |
| pGEX4T-2-human OGT | This paper | N/A |
| pET23C-human CREB | Huang et al., 2012 | N/A |
| Critical Commercial Assays | | |
| Cell Proliferation Kit II (XTT) | Sigma-Aldrich | Cat# 11465015001 Roche |
| TriZol reagent | Invitrogen | Cat# 1596018 |
| RNA extraction kit (ANbead Nucleic Acid extraction kit) | Taiwan Advanced Nanotech | Cat# M6K2A10 |
| Maxima First Strand cDNA Synthesis Kit | Thermo Fisher Scientific Inc. | Cat# K1642 |
| SYBR® FAST qPCR Kits | Kapa Biosystems | Cat# KK4603 |
| Herculase II fusion DNA polymerase | Agilent | Cat# 600677 |
| Deposited Data | | |
| Raw Tiff files for WB data | This paper | https://data.mendeley.com/datasets/stxrv6x98g/4 https://doi.org/10.17632/stxrv6x98g.4 |

(*Continued on next page*)

| Continued | | |
|---|---|---|
| REAGENT or RESOURCE | SOURCE | IDENTIFIER |
| Experimental Models: Cell Lines | | |
| HEK293T | ATCC | Cat# CRL-3216; RRID:CVCL_0063 |
| NSC-34 | A gift from Dr. Yijuang Chern (Academia Sinica, Taipei, Taiwan) (Cashman et al., 1992) | N/A |
| Experimental Models: Organisms/Strains | | |
| *C57BL/6-Gpx7$^{tm1Whle}$ (NPGPx$^{-/-}$)* | Wei et al., 2012 | MGI: 5473571 |
| Software and Algorithms | | |
| Prism 5 | GraphPad Software | https://www.graphpad.com/; RRID: SCR_002798 |
| ImageJ | National Institutes of Health | RRID: SCR_003070 |
| StepOnePlus Real-Time PCR System | Thermo Fisher Scientific Inc. | RRID: SCR_015805 |

## LEAD CONTACT AND MATERIALS AVAILABILITY

Further information and requests for resources and reagents should be directed to the Lead Contact, Wen-Hwa Lee (whlee@uci.edu). All unique/stable reagents generated in this study are available from the Lead Contact with a completed Materials Transfer Agreement.

## EXPERIMENTAL MODEL AND SUBJECT DETAILS

### Ethics Statement

Human samples were obtained from National Taiwan University Hospital (NTUH) and Taipei Medical University Hospital (TMUH). The samples were encoded to protect patient confidentiality. All patients signed an informed consent, which was approved by the Institutional Review Board of Human Subject Research Ethics Committee of National Taiwan University, Taipei Taiwan (IRB no. 201707039) and Joint Institutional Review Board of Taipei Medical University (IRB no. N201512017).

### Human Specimens

Peripheral blood from 33 ALS patients (15 females and 18 males) ranging in age from 37 to 73 years old, and 21 healthy controls (13 females and 8 males) ranging in age from 38 to 69 years old, were used for peripheral blood mononuclear cells (PBMC) isolation by Ficoll®-Paque gradient separation. The PBMC were subjected to RNA extraction followed by qPCR analysis to measure *NPGPx* and *GAPDH* expression levels.

### Animal protocols, generation of NPGPx-deficient mice, and mouse Thiamet-G treatment

All animal experiments were approved by the Institutional Animal Care and Utilization Committee of Academia Sinica, Taipei, Taiwan (IACUC#15-12-896). Unless specified otherwise, mice were maintained in a SPF (specific pathogen-free) animal facility at 20 ± 2°C with a 12/12 hr light/dark cycle and had free access to water and standard laboratory chow diet (LabDiet 5010). *NPGPx* knockout mice were generated and maintained as described previously (Wei et al., 2012). Briefly, the NPGPx-KO targeting vector was electroporated into E14 embryonic stem cells in 129/Ola background, and the correct ES cell was microinjected into C57BL/6J blastocytes. Chimeric mice were backcrossed with C57BL/6J mice for one generation to obtain heterozygous F1 offspring with germline-transmitted disrupted NPGPx allele. The mouse strain was maintained in C57BL/6J x 129/Ola mixed background by intercrossing of heterozygous mice. Homozygous *NPGPx* knockout (*NPGPx*$^{-/-}$) mice and wild-type littermates (*NPGPx*$^{+/+}$) in C57BL/6J x 129/Ola mixed background were obtained by intercross of F10 heterozygotes and used in most of the animal experiments unless particularly emphasized. For generating C57BL/6J congenic mice, *NPGPx*$^{+/-}$ mice in C57BL/6J x 129/Ola mixed background were backcrossed to C57BL/6J background for twelve generations. C57BL/6J congenic homozygous *NPGPx* knockout (*NPGPx*$^{-/-}$) mice and wild-type littermates (*NPGPx*$^{+/+}$) were obtained by intercross of F12 heterozygotes. For the Thiamet-G (MD08856, Carbosynth) treatment experiments, the age-matched mice were randomly divided into each experimental group (n = 10∼11 for each group). The mice were treated with Thiamet-G orally (100 mg/kg) at the age of 9 months to 12 months once every two days. All the mice in these experiments were female.

### Sample size estimation

Sample sizes were selected based on those commonly used in this field without predetermination by statistical methods as stated in the figure legends.

### General cell culture, lentiviral infection, and plasmid transfection

The HEK293T cell line was obtained from American Type Culture Collection and the mouse motor neuron-like hybrid cell line (NSC-34) produced by fusion of motor neuron-enriched embryonic mouse spinal cord cells with mouse neuroblastoma (Cashman et al., 1992) was obtained from Dr. Yijuang Chern (Academia Sinica). HEK293T and NSC-34 cells were cultured in Dulbecco's modified Eagle's medium (DMEM) supplemented with 10% FBS and antibiotics (penicillin/streptomycin). The cell lines were regularly checked for mycoplasma infection. For lentiviral infection, NSC-34 cells were plated in 10-cm dishes to 30% confluence and infected with lentiviral particles expressing the indicated plasmid. To establish the cell line that stably expresses the empty control vector (shEmpty) or shRNA against Luciferase, NPGPx, or OGA, NSC-34 cells were infected with the lentivirus containing the indicated shRNA. The infected cells were selected with 0.5 μg/ml puromycin for 2 days and passaged once without drug selection for further experiments. To establish the cell line that stably expresses the $NPGPx^{WT}$ or $NPGPx^{C2S2}$, NSC-34 shNPGPx cells were infected with the lentivirus containing the indicated cDNA. The infected cells were selected with 0.5 μg/ml hygromycin for 2 days and passaged once without drug selection for further experiments. To establish the cells that transiently expresses the HA-$NPGPx^{WT}$, HA-$NPGPx^{C2A2}$, Flag-OGA, HEK293T cells were transfected with plasmid DNAs containing indicated cDNA using TransIT-LT1 (Mirus) following the manufacturer's protocol.

## METHOD DETAILS

### Animal rotarod test and home cage analysis

For the rotarod test, WT and KO littermates were placed on an accelerating rotarod once per month from the age of 8 to 15 months. In the Thiamet-G treatment experiment, the rotarod test was performed at the age of 12 months. All mice were pre-trained twice a day for 4 consecutive days. For pre-trained trial, the mice were habituated to stay on the rod at 4 rpm constant speed for 60 s. On the day of testing, mice were kept in their home cages and acclimated to the testing room for at least 2 hr. For the testing phase, the mice were placed on the accelerating rod with the speed from 4 rpm to 40 rpm over a 300 s period for 3 test trials with 15 min inter-trial intervals. The latency to fall of each mouse was recorded. Rotarod data were collected by averaging three trials. For home cage analysis, the 15-month-old WT and KO littermates were placed individually in measuring cages for more than 16 hr before the formal experiment to habituate the animals to the experimental environment with free access to water and standard laboratory chow diet. On the day of testing, 60 g of chow food, 250 mL of RO water and 100 mL (30 g) of bedding were provided for each cage and mouse behavior was recorded by DVD encoder software for 1 hr. The behavior experiments were performed according to the manufacturer's instructions and protocol in the Taiwan Mouse Clinic.

### Plasmids and construction of expression plasmids

The pLAS3w-NPGPx WT and C2S2 were constructed by insertion of human *NPGPx* cDNA at *Nhe*I-EcoRI sites of the lentiviral cDNA expressing pLAS3w.Pbsd-L-tRFP vector (National RNAi Core Facility, Taiwan). The pcDNA 3.0-HA-NPGPx WT and C2A2 were constructed by insertion of human *NPGPx* cDNA at BamHI-*EcoR*I sites of the pcDNA 3.0-HA vector (Invitrogen). The Cys-to-Ser and Cys-to-Ala mutants of human *NPGPx* were generated using PCR-based site-directed mutagenesis (Herculase II fusion DNA polymerase, Ailgent) and confirmed by DNA sequencing. The pCMV-3xFlag 7.1-OGA was constructed by insertion of human *OGA* cDNA at SalI-*BamH*I sites of the p3xFlag-CMV™ 7.1 (Sigma-Aldrich). The pET-15b-OGA was constructed by insertion of human *OGA* cDNA at *Xho*I-*BamH*I sites of pET15b (Merck Millipore). The pGEX4T-2-OGT was constructed by insertion of human *OGT* cDNA at *BamH*I-SmaI sites of pGEX4T-2 (GE Healthcare). All the constructs were confirmed by DNA sequencing. The pET23C-human CREB was constructed as previous described (Huang et al., 2012). The pET48-TEV-human NPGPx WT and C2S2 (amino acids 19-187) were constructed as previous described (Wei et al., 2012). Small hairpin RNA (shRNA) plasmids for the mouse *NPGPx* gene (TRCN0000076564), mouse *OGA* gene (TRCN0000248909), and the empty control vector (pLKO-AS1) were obtained from the National RNAi Core Facility (Academia Sinica, Taipei, Taiwan). The target sequence for mouse *NPGPx* and *OGA* were 5′-CCT TCGGAAACGAGAAGACTT-3′ and 5′-TATACTATCAGACCTTATTTC-3′, respectively.

### Tissue preservation, immunohistochemistry, and image analysis

The mice were perfused with 4% (wt/vol) PFA in PBS (pH 7.4), and their L3-L5 lumbar spinal cords, their brains, and their hindlimb gastrocnemius muscles were collected. The tissues were further post-fixed overnight at 4°C. For immunofluorescence, lumbar spinal cords were osmotically dehydrated in 30% sucrose solution (in PBS, pH 7.4) for more than 36 hr at 4°C. After embedding in optimal cutting temperature compound (OCT compound), spinal cords and brains were sectioned into 20 μm thick slices using a cryostat (Leica Biosystems). Immunofluorescence was performed using sections mounted on adhesive slides. The sections were blocked in PBS containing 3% BSA, 5% FBS and 0.3% Triton X-100 for 30 mins and then briefly washed with PBS. Antibodies were diluted in PBS containing 3% BSA and 0.1% Triton X-100, and then applied to sections for 2 days at 4°C. Sections were washed with PBS and incubated for 120 mins at room temperature with fluorochrome-conjugated secondary antibodies (Biotium). For detecting NMJ architecture, the gastrocnemius muscles were teased into layers of 5-10 fibers in thickness for staining. The muscles were blocked with 3% BSA, 5% FBS, 0.5% Triton X-100 in PBS for 30 mins and then briefly washed with PBS. The muscles were incubated with the anti-NF-200 (1:100, Abcam, ab8135) against presynaptic nerve terminals and α-Bungarotoxin-Alexa 594 (1:500, Invitrogen, B-13423) against acetylcholine receptors (AChRs) in PBS containing 3% BSA and 0.1% Triton X-100 at 4°C for 2 days. The muscles were

washed with PBS and incubated for 120 mins at room temperature with fluorochrome-conjugated secondary antibodies (Biotium). All images were acquired using a SP5 or SP8 confocal microscope (Leica Microsystems). For the ChAT-positive motor neuron (MN) counts, MN were defined and counted according to the following criteria: (1) > 25 μm in size; (2) Location in ventral gray matter regions below a horizontal level through the center of the central canal. For quantification of GFAP, CD11b, *O*-GlcNAc, p-eIF-2α and DHE intensities, the images were acquired using identical confocal settings, and then analyzed quantitatively using ImageJ. For NMJ innervation analysis, more than 50 endplates were evaluated from each group of mice. The NMJ was evaluated by categorizing endplates as fully innervated (neurofilament signal labeling of more than 80% of the endplate), partially innervated (neurofilament signal labeling from 10% to 80% of the endplate), and fully denervated (neurofilament signal labeling less than 10% of the endplate).

### Nissl staining

Spinal cord frozen sections (20 μm in thickness) were hydrated with Xylene, 95% alcohol, and 70% alcohol for 3 min each step and stained with cresyl violet solution (containing 0.13% cresyl violet, 85 mM acetic acid, and 5.5 mM sodium acetate) for 8 min at 60°C. The stained sections were washed with distilled water for 3 min, and then dehydrated with 70% alcohol, 95% alcohol, and 100% alcohol sequentially. The sections were then fixed in xylene and coverslipped with Xylene based mounting media. The Nissl-stained cells larger than 25 μm in size and located in ventral gray matter regions below a horizontal level through the center of central canal were defined as MN.

### Generation of NPGPx-specific monoclonal antibody

For generation of NPGPx-specific monoclonal antibody (7E7-3B2), recombinant human NPGPx protein (aa 19-187) was used as immunogen to immunize BALB/c mice. The spleen cells from successful immunized mice were fused with myeloma cells to obtain antigen-specific hybridomas.

### *In situ* proximity ligation assay

The cells were fixed with 3.7% formaldehyde and permeabilized with 100 μg/ml digitonin for 10 min at RT for each step. The slides were further blocked with PBS containing 1% BSA for 30 min at RT and incubated with primary antibodies (mouse anti-NPGPx (clone 7E7-3B2; this paper), rabbit anti-OGA (SAB4200267; Sigma), and goat anti-calnexin (ab192439; Abcam)) overnight at 4°C. The slides were washed with 1% BSA in PBS containing 0.05% Triton X-100 for 10 min three times, and then incubated with PLA anti-Rabbit PLUS probe (Sigma) as well as PLA anti-Mouse MINUS probe (Sigma) for 1 hr at 37°C. The hybridization and ligation steps were performed using the Duolink® *In Situ* Fluorescent Detection Reagent-FarRed (Sigma) according to the manufacturer's instructions. The slides were then stained with Alexa Fluor® 488 conjugated donkey anti-goat IgG (A11055; Invitrogen) for 1 hr at RT. Afterward, the slides were stained with DAPI and mounted with Fluorescence Mounting Medium (Dako), and then imaged with a Zeiss LSM880, 63x objective (Carl Zeiss AG, Germany). PLA dot numbers were counted by ImageJ (National Institutes of Health).

### Enzymatic activity assay

#### *O-GlcNAc transferase activity assay –*

The NSC-34 cells or spinal cords were lysed in lysis buffer containing 50 mM Tris-Cl, pH 7.5, 1 mM EDTA, 270 mM sucrose, and 1% Triton X-100 for further analysis. Equal amounts of cell lysate (100 μg per assay) were applied to the reaction mixture containing 25 mM HEPES, pH 7.5, 10 mM $MgCl_2$, 1 mM EDTA, 2.5 mM AMP, 0.5 μCi of UDP-[$^3$H]-GlcNAc, and 10 μg CREB at 25°C for 2 hr. The reaction (100 μL each) was stopped by adding 200 μL of cold 15% trichloroacetic acid. After cooling down on ice for 10 min, the mixtures were centrifuged at 16000*g for 30 s, and the pellets were washed with 10% trichloroacetic acid twice. The precipitated pellets were resuspended in 150 μL of 0.5% SDS. The dissolved samples were applied to the scintillation counter for detecting radioactivity transferred on CREB.

#### *O-GlcNAcase activity assay –*

The NSC-34 cells or spinal cords were lysed in lysis buffer containing 50 mM sodium phosphate, pH 7.0, 150 mM NaCl, and 0.1% NP-40. Equal amounts of cell lysate (80 μg/assay) or recombinant proteins were introduced into the reaction mixture (100 μl/assay) containing 50 mM sodium phosphate (pH 6.5), 100 mM NaCl, 2 mM para-Nitrophenyl-N-acetyl-β-D-GlcNAc (Sigma, N9376), and 1 mM GalNAc (Sigma, A3795) at 37°C for 1 hour. The reactions were stopped with 100 μL sodium carbonate (0.5 M), and absorbance at 405 nm was measured.

### Co-immunoprecipitation (Co-IP) and Western analysis

Tissue homogenates or cell lysates were prepared using NP-40 lysis buffer containing 20 mM sodium phosphate (pH 7.0), 150 mM NaCl, 2 mM EDTA, 0.5% NP-40, 0.1% SDS, 0.5% deoxycholic acid, protease inhibitor mixture (Roch Applied Science) and phosphatase inhibitor cocktail (Tools, TARR-WBC1). For Co-IP, 1 mg of the crude whole-cell extract was incubated with 1 μg target protein antibodies or control IgG at 4°C for 2 hr. Then, 50 μL prewashed protein A/G agarose (Thermo) were added to the mixture and incubated at 4°C for additional 2 hr with gentle agitation. For precipitation of HA- or Flag-tagged proteins, 20 μL anti-HA or M2 beads (Sigma), respectively, were used to precipitate target proteins from crude whole-cell extract. Beads were washed three times with NP-40 lysis buffer, and immunoprecipitated proteins were eluted with Laemmli sample buffer with or without reducing agent, 2-mercaptoethanol (2-ME). Protein samples resolved by SDS-PADE were transferred to PVDF membrane, and the then incubated with

primary antibody followed by horseradish peroxidase (HRP)-conjugated IgG secondary antibodies (1:10,000, Jackson ImmunoResearch). Signals were detected using Immobilon Western Chemiluminescent HRP Substrate (Merck Millipore, WBKLS0500). The intensity of each band in immunoblotting was quantified using the ImageJ software. The levels of *O*-GlcNAcylation, p-p38, and p-eIF-2$\alpha$ were normalized to tubulin, p38, and eIF-2$\alpha$, respectively.

### Recombinant protein preparation and *in vitro* protein binding assay

N-terminally His-tagged OGA, His-tagged OGT and GST-tagged OGT were produced in *E. coli* via 0.4 mM IPTG induction at 16°C overnight. Purification was conducted via affinity chromatography on a column composed by Ni-NTA agaroses (GE Healthcare Life Sciences) or Glutathione agaroses (Thermo). Recombinant NPGPx protein was purified as described previously (Wei et al., 2012). To prepare reduced or oxidized NPGPx, OGA, and OGT, the procedure was performed as previously described (Wei et al., 2012). In brief, the proteins were treated with 10 mM Tris(2-carboxyethyl)phosphine (TCEP) or 1 mM $H_2O_2$, respectively, for 1 hr at 4°C. The TCEP and $H_2O_2$ were removed by buffer (50 mM Tris, pH 7.5, 100 mM NaCl, 5% glycerol) exchange using centrifugal ultrafiltration devices. 1 $\mu$M of OGA or OGT and 40 $\mu$M of NPGPx with different redox statuses were incubated together at 25°C for 2 hr and then subjected to SDS-PAGE analysis with or without reducing agent (2-ME) followed by western blotting. GST pull-down analysis was performed as described previously (Huang et al., 2012). In brief, 2 $\mu$g GST or GST-OGT proteins were incubated with NPGPx recombinant protein. After binding and washing, bound proteins were subjected to western blot analysis.

### ROS level measurement *in vitro* and *in vivo*

For ROS determination in NSC-34 cells under $H_2O_2$ stimulation, the cells were treated with or without 1 $\mu$M Thiamet-G for 4 hr before staining with CM-$H_2$DCFDA (Invitrogen, C6827) for 20 mins. The stained cells were stimulated with $H_2O_2$ for an additional 3 hr in the presence or absence of Thiamet-G. The stained cells were subjected to FACS analysis by Canto II flow cytometry (BD Bioscience). For detection of ROS generation in spinal cords and brain tissues, mice were injected (i.v.) with dihydroethidium (DHE) (Invitrogen, D11347) at 0.05 mg/g body weight per mouse. After 4 hr, the mice were perfused with PFA and the tissues were sampled as described above.

### Cell viability assay

To measure the viability of $H_2O_2$-treated NSC-34 cells, $1 \times 10^4$ cells per well were seeded in flat-bottom 96-well plates. After 16 hr, the cells were pretreated with Thiamet-G (1 $\mu$M) for 4 hr and then treated with the indicated concentration of $H_2O_2$ for 3 hr with or without TMG (1 $\mu$M). After PBS washing three times, the cells were maintained in fresh complete medium with or without Thiamet-G (1 $\mu$M) for an additional 16 hr incubation. Cell viability was determined by XTT Assay Kit (Sigma, 11465015001 Roche) according to the manufacturer's protocol.

### RNA extraction, reverse transcription and real-time qPCR

To quantify *NPGPx* gene expression in the PBMC from ALS patients and healthy controls, the PBMC were resuspended in TriZol reagent and subjected to RNA extraction using an RNA extraction kit (TANbead Nucleic Acid Extraction Kit, Taiwan Advanced Nanotech). The RNA was reverse-transcribed into cDNA using the Maxima First Strand cDNA Synthesis Kit (Thermo Fisher Scientific Inc.). The cDNA was subjected to real-time PCR using SYBR® FAST qPCR Kits (Kapa Biosystems) and StepOnePlus Real-Time PCR System (Thermo Fisher Scientific Inc.). The *GAPDH* expression level served as an endogenous control for normalization. Primer information is described below:

*NPGPx*-forward: 5′-GCAGGAGCAGGACTTCTACGACTTC-3′,
*NPGPx*-reverse: 5′-ACCGGTGACTGCAATCTTGCTAAAC-3.
*GAPDH*-forward: 5′-GGCTCTCCAGAACATCATCCCTGC-3′,
*GAPDH*-reverse: 5′-GGGTGTCGCTGTTGAAGTCAGAGG-3′.

### Experiment design

#### *Replication*

All experimental findings were reproduced in multiple independent experiments.

For each figure panel, the number of independent experiments or biological replicates is indicated in the figure legends. Data shown in figure panels are the mean ± s.e.m. or mean ± s.d. of all independent biological or technical repeats as indicated in the figure legends. Western blot images are from a representative experiment and the number of independent repeats is clearly indicated in the figure legends.

#### *Strategy for randomization and/or stratification*

The age-matched mice with similar body weight were randomly divided into each experimental group. This is stated in the ''Animal protocols, generation of NPGPx-deficient mice, and mouse Thiamet-G treatment.''

#### *Blinding at any stage of the study*

The investigators were blinded to the group allocation during experiments and outcome assessment.

### *Sample-size extermination and statistical method of computation*

We chose our sample sizes based on those commonly used in this field without predetermination by statistical methods. This is stated in the figure legends. For all figures and tables that use statistical methods, we confirmed that the following items are present in relevant figure legends.

1. The exact sample size (n) for each experimental group/condition, given as a discrete number and unit of measurement (animals, litters, cultures, etc.)
2. A description of how samples were collected, noting whether measurements were taken from distinct samples or whether the same sample was measured repeatedly.
3. A statement indicating how many times each experiment was replicated.
4. The statistical test(s) used and whether they are one- or two-sided. Only common tests should be described solely by name; describe more complex techniques in the STAR Methods section.
5. A description of any assumptions or corrections, such as an adjustment for multiple comparisons
6. Test values indicating whether an effect is present. Provide confidence intervals or give results of significance tests (e.g., *P value*s) as exact values whenever appropriate and with effect sizes noted.
7. A clear description of statistics including central tendency (e.g., median, mean) and variation (e.g., standard deviation, interquartile range).
8. Clearly defined error bars in all relevant figure captions (with explicit mention of central tendency and variation)

### *Inclusion and exclusion criterial of any data or subjects*

All samples/ animals that met proper experimental conditions were included in the analysis. No data were excluded from the analyses.

## QUANTIFICATION AND STATISTICAL ANALYSIS

### Statistical Analyses

All statistical tests were analyzed by two-tailed t test for comparison of two groups or by analysis of variance (ANOVA) using GraphPad Prism 5.0. Except for the animal experiments, all data were presented as means ± s.d., and Student's t test (two-tail, unpaired) was used to ascertain the statistical significance between control and experimental groups. * indicated statistical significance with $p < 0.05$ and ** indicated statistical significance with $p < 0.01$. Data distribution was assumed to be normal. The variance was similar between the groups that were being statistically compared (by F-test). For the animal experiments, data were presented as mean ± s.e.m.. The variance between the groups was ascertained statistically by F-test. If the variance was similar between the groups, the data were analyzed by two-tailed Student's t test for comparison of two groups. Otherwise, the data were analyzed by unequal variances test (Welch's test) for comparison of two groups. N number used in indicated section was shown in the figure legends.

## DATA AND CODE AVAILABILITY

Raw Tiff files for WB data had been deposited in Mendeley:
https://data.mendeley.com/datasets/stxrv6x98g/4
https://doi.org/10.17632/stxrv6x98g.4
The information for ImageJ and Prism 5 software are included in the Key Resources Table.